



## Comparison of QuikSCAT, WRF and buoy ocean surface wind data off Valparaiso Bay, Chile



M. Cáceres-Soto<sup>a,b,\*</sup>, H.H. Sepúlveda<sup>c</sup>, K. Muñoz-Mellado<sup>c</sup>, O. Artal<sup>d</sup>

<sup>a</sup> Programa de Magister en Oceanografía, Escuela de Ciencias del Mar, Pontificia Universidad Católica de Valparaíso, Valparaíso, Chile.

<sup>b</sup> Chilean Navy Hydrographic and Oceanographic Service, Valparaíso, Chile

<sup>c</sup> Geophysics Department, University of Concepcion, Concepcion, Chile

<sup>d</sup> Departamento de Medioambiente, Instituto Fomento Pesquero, Castro, Chile

### ARTICLE INFO

#### Keywords:

Winds  
Buoy  
Chile  
QuikSCAT  
ERA-Interim  
WRF

### ABSTRACT

The winds that affect the surface of the ocean are also important for a vast array of activities, either operational or scientific, hence the importance of being able to adequately predict this quality. Because of the preceding fact, a Weather Research and Forecasting model was used to perform simulations at the surface of the Ocean, for winds derived from different boundary conditions (NCEP-CFSR, ERA-Interim and NCEP-FNL) and configured with different spatial resolution (25, 5 and 1 km), with the objective of evaluating which of these data sets delivers the more precise wind simulation at the surface of the ocean.

A comparative analysis was performed between the different outputs of the WRF model, QuikSCAT satellite and *in situ* observations of a buoy installed off the central coast of Chile. The results showed that the WRF model, overestimates the wind magnitudes, across all boundary conditions or spatial resolution. Additionally, depending on the *in situ* wind magnitude ( $> 6 \text{ ms}^{-1}$ ), the model predicts adequately wind magnitude and direction. Spatial comparisons were performed between QuikSCAT and WRF outputs at the Chilean coast to evaluate any possible differences. The modeled winds showed a tendency to be stronger than those measured by Satellites and the bigger differences appeared closer to the shore. The wavelet coherence and phase analysis, confirmed that the model delivers precise wind information for frequencies greater than the daily cycle. Finally, the results of the simulation produced by the ERA-Interim analysis showed lower errors in terms of temporal and spatial variability of surface winds.

### 1. Introduction

The winds that affect ocean surfaces and coastal areas have significant impact on diverse activities, such as fishing, tourism, port operations, commercial navigation and recreational sailing. The upwelling is a characteristic process forced by the surface wind on the Chilean-Peruvian coast. Upwelling zones play an important role for the global climate system, since they are areas of high primary productivity with considerable biological capture of atmospheric carbon (Aguilera et al., 2009). This upwelled water is normally cold, rich in nutrients and  $\text{CO}_2$ , and poor in oxygen. This primary production due to the nutrient stimulus in the euphotic zone will tend to balance or even reverse the air-sea fluxes of  $\text{CO}_2$  and  $\text{O}_2$  (Torres et al., 2002).

Winds also play an important role in ocean-atmosphere exchange, which is critical for meteorological and oceanographic studies because of the important role they play in processes like Ekman pumping (Capet

et al., 2004), subsurface currents (Aguirre et al., 2014) and wave formation (Stopa and Cheung, 2014). For example, a seasonal decrease in low-cloud cover produces peak coastal winds in the austral summer due to the greater thermal contrast land-sea (Rutllant et al., 2004).

Numerical atmospheric models are commonly used to predict surface winds at distinct spatial scales. Modeled wind fields are used as forcing agents in circulation (Renault et al., 2012) and wave models (Caires et al., 2004). Errors in modeling surface winds can affect the output of ocean models that use this variable as a forcing agent (Sousa et al., 2013), because of which its correct representation and validation by different methods is critical.

Numeric oceanic models have been validated by different instruments (Rutllant and Garreaud, 2005; Sánchez et al., 2007; Ruti et al., 2008; Balzarini et al., 2011; Purba et al., 2014) with different logistical complications. Oceanographic buoys are costly to maintain and operate, and can be affected by vandalism and adverse environmental

\* Corresponding author at: Programa de Magister en Oceanografía, Escuela de Ciencias del Mar, Pontificia Universidad Católica de Valparaíso, Valparaíso, Chile.  
E-mail address: [mario.caceres.s@mail.pucv.cl](mailto:mario.caceres.s@mail.pucv.cl) (M. Cáceres-Soto).

conditions. As well, *in situ* measurements in discrete points in space do not necessarily represent large or medium-scale wind regimes (Risien and Chelton, 2006). However, a long sampling period can allow for determining the temporal variability of meteorological and oceanographic processes. As well, there is no effect of coastal topography further from the continent.

There have been few *in situ* measurements of the Southeastern Pacific Boundary System along the Chilean coast compared to those of the other eastern boundary systems (Bakun and Nelson, 1991). The oceanic area along the Chilean coast is dominated by a semi-permanent high pressure system known as the South Pacific Anticyclone (SPA), which produces stable conditions in the lower troposphere at 18° to 42° S, with winds predominantly from the south, and low sea temperatures owing to upwelling, mainly in spring and summer (Letelier et al., 2009). The SPA has seasonal cycles, shifting to approximately 35°S in the summer and being more intense along the southern coast of Chile, while in winter they are more intense around 30°S in northern Chile (Ancapichún and Garcés-Vargas, 2015). Seasonal wind patterns have low variability between 18° and 28° S (Pizarro et al., 1994), while winds south 30° S show marked seasonality and are more intense than winds north of this line (Garreaud and Muñoz, 2005).

Winds are more intense in winter and spring because this is when the SPA is directed more toward the equator, which results in vertical compacting of the air mass and an increase in the pressure gradient (Pezza et al., 2007). Winds in the lower troposphere are strongly affected by topographic characteristics and vegetation patterns in the continent, the Andean Mountain Range being a significant barrier to atmospheric circulation in the troposphere (Garreaud and Aceituno, 2001). The influence of the SPA at Chile generates permanent equatorward winds determining the water mass composition and the phytoplankton biomass of the coastal waters. The dynamics of phytoplankton governed by successive upwelling events (Torres et al., 2002), leading to dominance of chain-forming diatoms, interrupted by small size and flagellated cells during warm conditions of the water column (Herrera and Escribano, 2006).

Several authors have characterized the surface wind regime along the Chilean coast using remote sensing (Garreaud and Muñoz, 2005; Muñoz, 2008). The QuikSCAT satellite allows for observing the surface wind field and provides two measurements per day at a spatial resolution between 12.5 and 25 km, which can present data gaps (Carvalho et al., 2014). Studies assessing the precision of QuikSCAT-derived wind data (Tang et al., 2004; Ruti et al., 2008) have indicated a low yield owing to heavy rains that artificially increase surface roughness and low intensity winds ( $< 5 \text{ ms}^{-1}$ ). Information on the near coastal area is generally omitted because of the masking effect of the land, which does not allow for representing the temporal-spatial variability of coastal winds.

The lack of data about winds close to the coast can be offset by mesoscale atmospheric models (Luo et al., 2008). However, these models can present discretization problems related to complex local topography, and the discontinuity and thermal gradients between land and sea (Bengtsson et al., 2007). Among the advantages of this model are the versatility of its temporal and spatial resolution, which allows for simulating atmospheric dynamics. However, it is critical to validate the temporal and spatial variability of atmospheric models.

Adequate configuration, in particular in relation to boundary conditions, is necessary to obtain good results from a mesoscale atmospheric model of a particular area. These conditions are generally obtained from analysis or re-analysis, which provides the necessary atmospheric information to force mesoscale models. Several studies have investigated the accuracy of mesoscale atmospheric models and compared them to satellite wind data simulations and *in situ* ocean surface measurements, with satisfactory results (Otero and Ruiz-Villareal, 2008; Penabad et al., 2008; Wallcraft et al., 2009; Carvalho et al., 2013). The best results for ocean areas are usually provided by numerical weather prediction models (NWP), although coastal winds

continue to be a challenge for numerical modeling and remote sensing.

The objective of this work is to assess ocean surface winds on the coast of central Chile using the atmospheric model Weather Research and Forecasting (WRF, Skamarock et al., 2008), based on different boundary conditions (global analysis and reanalysis). The results of the WRF model were compared to *in situ* and satellite measurements to determine the best boundary condition to simulate winds along the coast of central Chile using the WRF model.

## 2. Materials and methods

This study used ODAS buoy and satellite data and the results of a numerical atmospheric model forced by boundary conditions with distinct global atmospheric data (analysis and reanalysis) at different spatial resolutions. The different information sources and the statistical criteria used to compare them are described below.

### 2.1. Buoy data

The Watchkeeper Buoy (WKB) is an oceanographic and meteorological data measurement platform anchored off Valparaíso Bay (71° 49' 48" W, 32° 59' 34" S), around 20 km west of Punta Ángeles and 15 km from the coast at a depth of 486 m (Fig. 1). It is without any protection against winds and waves. The buoy is 4 m high and weighs 600 kg. The upper part has instruments for obtaining meteorological data. The buoy serves to support the Chilean Navy's weather forecasting system and is operated by the Navy Hydrographic and Oceanographic Service.

The WKB measures wind hourly at a height of 3 m. Wind data are obtained from an average of measurement results for approximately 10 min every hour results. With the aim of comparing the data series, the wind magnitude data provided by the meteorological buoy were adjusted to a height of 10 m by means of the COARE v3.0 (Fairall et al., 2003), in which the bulk parametrizations calculate the heat sensitive and latent exchange flows using wind intensity, air and sea temperature and differences in specific humidity.

The data cover the period from August 21 (installation of the WKB) to November 21, 2009 (last days of available QuikSCAT data). There were few and brief data gaps, representing 0.14% in total. Gaps in the records of less than 3 h were filled with linear interpolation, while longer gaps were interpolated by least squares harmonic adjustment.

### 2.2. Satellite data (QuikSCAT ocean surface winds)

The NASA SeaWinds instrument, which is on board the QuikSCAT satellite, was designed with the purpose of mainly measuring ocean surface winds at a height of ten meters above sea level. The satellite was launched in July 1999 and stopped operating in November 2009. The satellite was equipped with a microwave disperometer that measured ocean roughness. The data was provided in two spatial resolutions (25 and 12.5 km), with two measurements daily, which in the case of the area of this study were at 11 am and 11 pm during the ascending and descending passes, respectively. More information on the satellite can be found in the webpage of the NASA's Physical Oceanography Distributed Active Archive Centre at the Jet Propulsion Laboratory <http://podaac.jpl.nasa.gov/OceanWind/QuikSCAT>.

The QuikSCAT satellite is recognized to have low yield under adverse weather conditions like strong rains and low intensity winds (Tang et al., 2004; Ruti et al., 2008; Pensieri et al., 2010). Fore et al. (2013) developed the high resolution V3L2B12 product (12.5 km), which has demonstrated less noise in wind intensity and direction than earlier products. Among its other advantages are fewer gaps at 12.5 km, a neuronal network to eliminate contamination caused by rain and the extraction of bias. This last information was used for this research study.

The study area selected to compare buoy and satellite data is

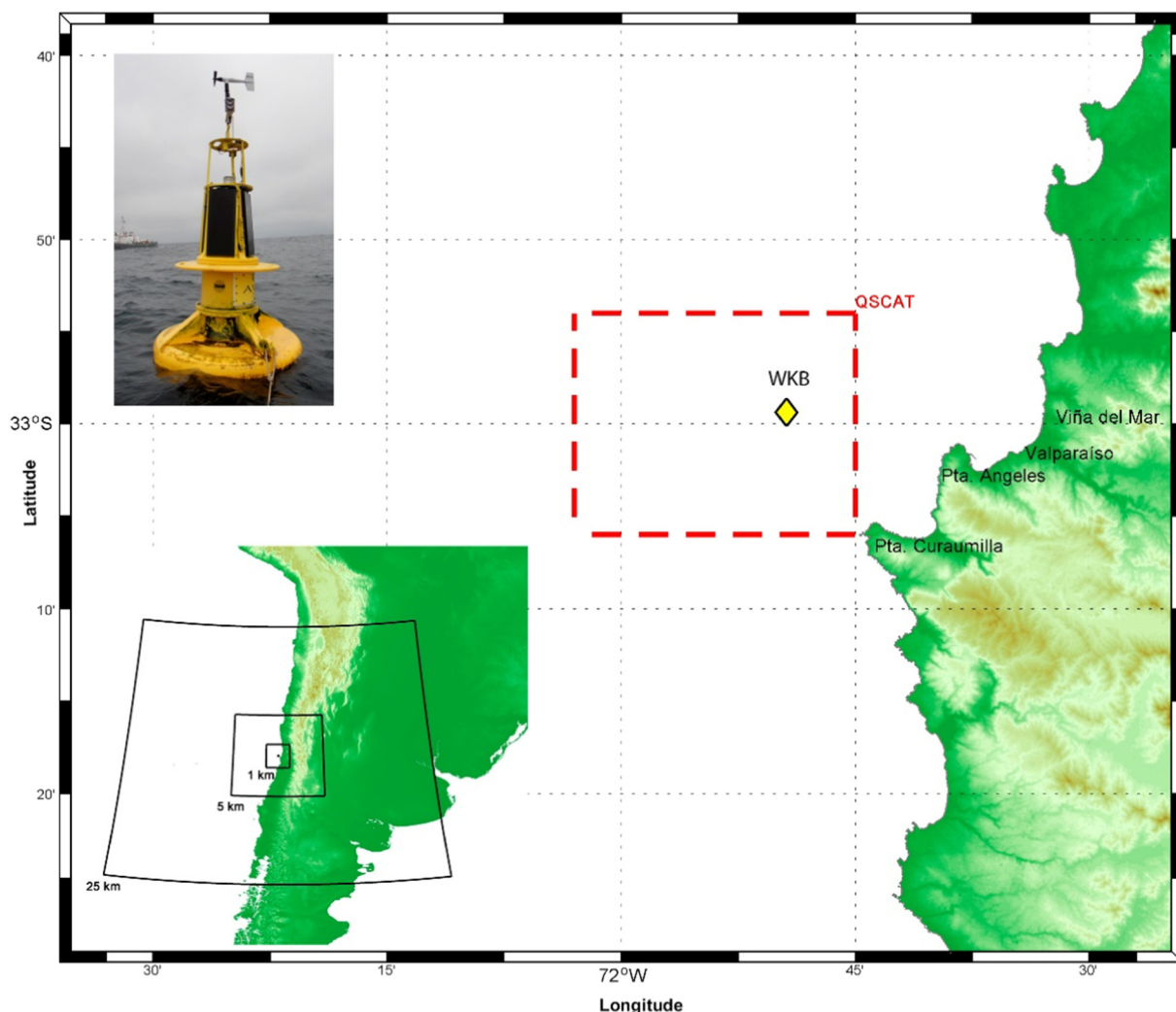


**Fig. 1.** Map of the study area (central Chile). The yellow diamond represents the position of the WKB. The area inside the dashed red lines is covered by the satellite data used in the study. The numerical grids used in this study are shown in the lower left of the image. (For interpretation of the references to colour in this figure legend, the reader is referred to the web version of this article.)

between 32.9 and 33.1°S, and 71.75 and 72.05°W. The area is shown in red in Fig. 1.

**2.3. Mesoscale atmospheric modeling (WRF)**

The numerical model WRF (Skamarock et al., 2008) is a latest generation non-hydrostatic mesoscale model that is widely used for operative weather forecasts and researching meteorological phenomena.

The WRF model has a configuration of three nested domains in a ratio of 1 to 5. The largest domain (Grid No 1), covers much of Chile (86.8–57°W, 43.9–21.4°S), with a horizontal spatial resolution of 25 km. The intermediate-sized domain (Grid No 2), covers central Chile (75.9–67.8°W, 36.5–29.5°S), with a spatial resolution of 5 km, while the smallest domain (Grid No 3), has a resolution of 1 km (Fig. 1). All the domains are centered on the position of the WKB. Spatial resolutions of 5', 2', 30' of arc, respectively, were used for the topographic data. On the vertical, twenty-eight levels of pressure and Lambert-type projection were used in the vertical. The largest grid reproduces the large-scale synoptic characteristics that force the dynamics of the other domains. The model generates winds at 10 m above the ocean surface. Table 1 summarizes the physical parameters used in the model.

The Climate Forecast System Reanalysis (NCEP-CFSR, <http://cfs.ncep.noaa.gov/cfsr/>, Saha et al., 2010) is the only dataset in this study

**Table 1**  
Summary of the physical WRF parametrizations (all the domains).

Microphysics	WRF single moment 5-class scheme
Cumulus	Kain-Fritch
Longwave	Rapid Radiative Transfer Model scheme
Shortwave	Goddard scheme
PBL scheme	YSU scheme
Surface physics	Noah scheme
Surface layer	Monin Obukhov scheme

that uses ocean-atmosphere coupling between the ice and the sea surface. It has a spatial resolution of 0.5° by 0.5°, with 40 vertical levels and assimilates irradiance by satellites. Another reanalysis dataset is ERA-Interim, developed by the European Centre for Medium-Range Weather Forecasts (ECMWF), which assimilates four-dimensional variational data (4D-Var) with BIAS correction in the radiance observations by satellite (Dee et al., 2011). Its spatial resolution is 0.75° by 0.75° distributed in 60 vertical levels. The NCEP-FNL dataset, with one degree by one degree grids, comes from the NOAA Global Forecasting System (GFS, <http://weather.rap.ucar.edu>). It is different from the other datasets in that it is an analysis and not a reanalysis. All these products have a 6-hour temporal resolution.

The sea surface temperature (SST) entered into the WRF model for

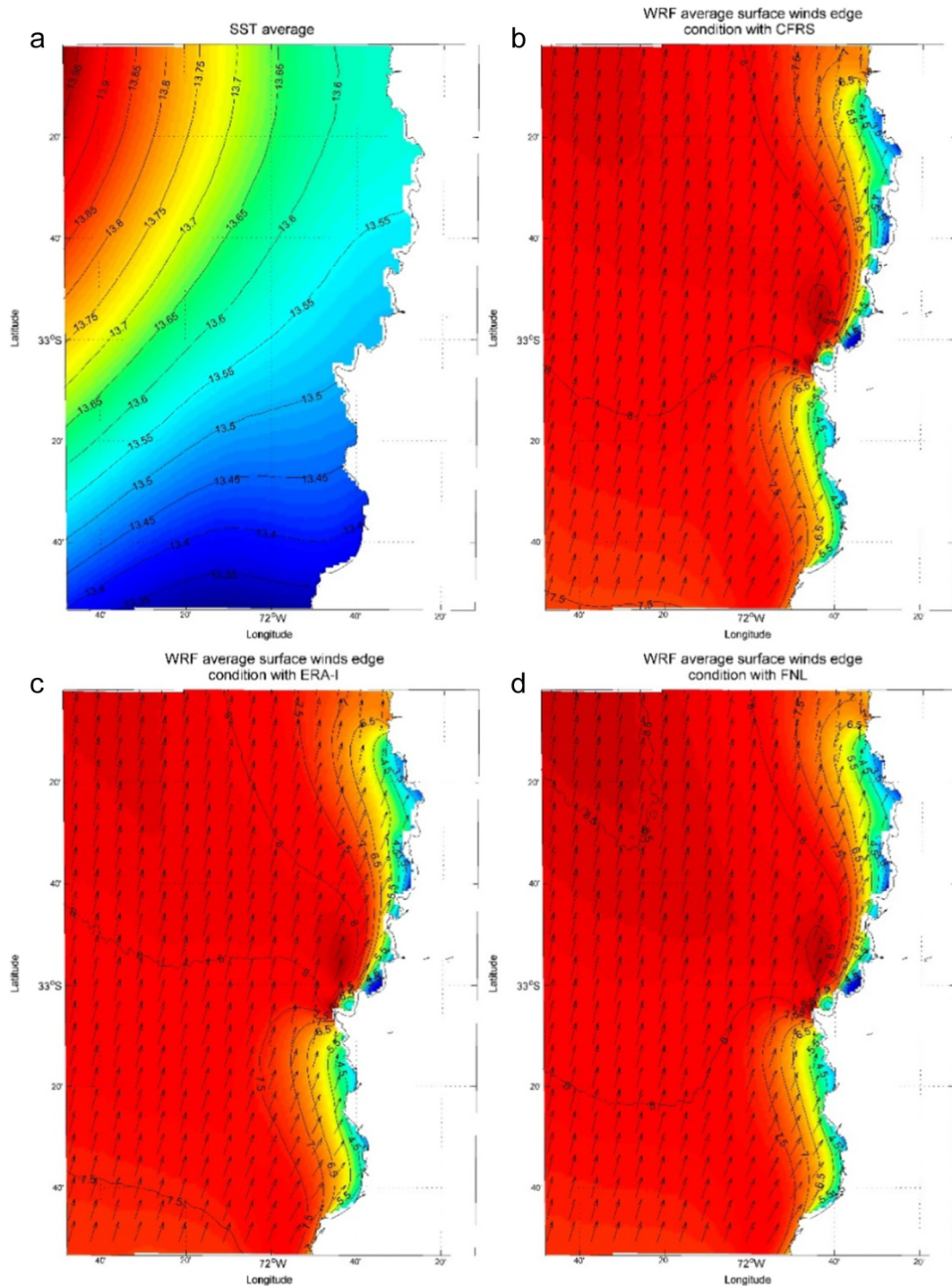


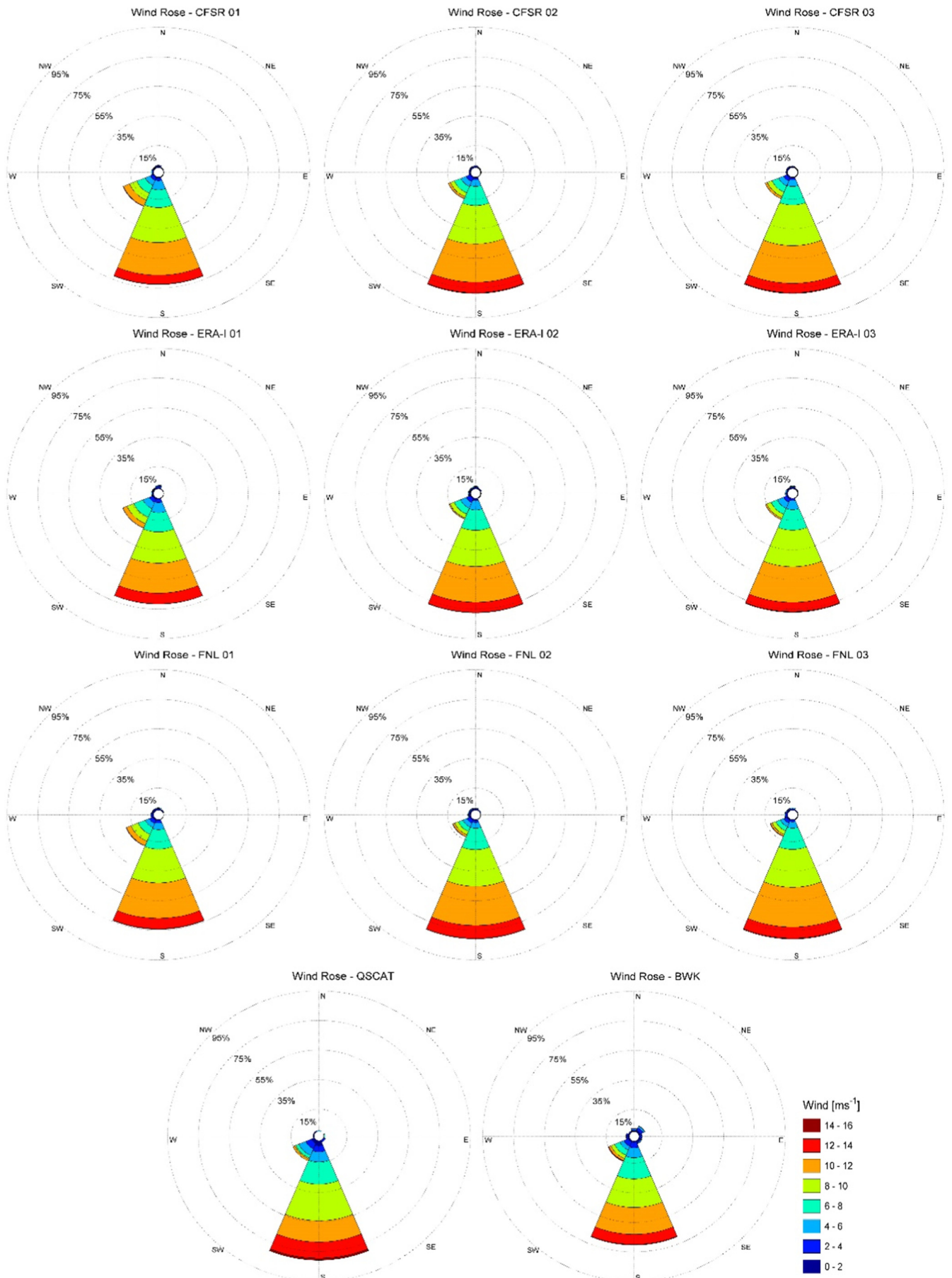
**Fig. 2.** a) SST average and simulations of average surface wind of different condition boundary conditions of b) NCEP-CFRS, c) ERA-Interim and d) NCEP-FNL.

the three different edge conditions (NCEP-CFSR, ERA-INTERIM and NCEP-FNL) corresponds to that modeled by NCEP-NOAA ([ftp://polar.ncep.noaa.gov/pub/history/sst/rtg\\_low\\_res](ftp://polar.ncep.noaa.gov/pub/history/sst/rtg_low_res)), with a daily time resolution and a spatial resolution of  $1^{\circ} \times 1^{\circ}$ . The SST period average (Fig. 2a), a slight temperature difference is observed between the coastal edge and the most oceanic sector, evidencing a lower temperature along the coast, with values of  $13.55^{\circ}\text{C}$  and a higher offshore temperature, which they reach values of  $13.95^{\circ}\text{C}$ . SST evidences that the edge conditions are able to characterize the coastal upwelling produced by the winds coming from the south, driven SPA anticyclone of the Pacific, as shown in the average wind figures for each edge

condition.

Regarding the averages of the surface wind fields of the edge conditions used, it is observed that they are similar magnitudes, which range between  $3\text{ ms}^{-1}$  on the coast and  $8.5\text{ ms}^{-1}$  away from the coast. It is observed that the speed accelerates in the sector of Punta Curaumilla in all cases. Particularly with ERA-INTERIM (Fig. 2c) apparently the greatest magnitudes are concentrated around the latitude of  $33^{\circ}\text{S}$ .

The simulation covered a period of 3 months, from August 21 to November 21, 2009, with the objective of verifying the spatial-temporal variability and observing the operation of the model in the time-



(caption on next page)

**Fig. 3.** Roses of winds ( $\text{ms}^{-1}$ ) obtained from the WKB, WRF simulations with different boundary conditions and QuikSCAT data from August 21 to November 21, 2009.

frequency domain.

#### 2.4. Statistical evaluation of wind data

The statistical indicators root mean squared error (RMSE), BIAS and correlation coefficients (R) for wind magnitude and direction were used to compared wind measurement data from different sources. Only the data of the intensity and direction of the winds from all the databases were considered for these calculations to evaluate the performance of the products for the same point in time.

$$RMSE = \left[ \frac{1}{n} \sum_{i=1}^n (S_i - B_i)^2 \right]^{\frac{1}{2}} \quad (1)$$

$$BIAS = \frac{1}{n} \sum_{i=1}^n (S_i - B_i) \quad (2)$$

$$R_{S,B} = \frac{cov(S,B)}{\sigma_S \sigma_B} \quad (3)$$

where S is the WRF/QuikSCAT wind data and B is the WKB wind data. These calculations are generally trivial for scalar variables like wind magnitude. However, the methodology proposed by Berens (2009), which involves a series of scripts for directional data analysis, is used for circular variables like wind direction. Weibull probability density functions were used to characterize the distribution and frequency of wind intensity and compare the different databases. Weibull distribution has been used widely, because of its approximate adjustment to describe the distribution of wind intensity (Álvarez et al., 2014).

The variability of wind direction was analyzed based on the differences between the simulations and *in situ* measurements. Wind direction was modified in the following way to reduce the discontinuity between  $0^\circ$  and  $360^\circ$ :  $\theta_s = \theta_s - 360^\circ$  when  $\theta_s - \theta_b > 180^\circ$  and  $\theta_s = \theta_s + 360^\circ$  when  $\theta_s - \theta_b < -180^\circ$ , with  $\theta_s(\theta_b)$  being the wind direction of the simulations/satellite (buoy), as indicated in the methodology of Pensieri et al. (2010).

#### 2.5. Spatial analysis

The QuikSCAT satellite data and the output of the WRF model were compared spatially. The model covered the same area as covered by the satellite, with a resolution of 25 by 25 km. A grid was employed with dimensions of 98 by 55, covering an area of  $21^\circ 24'S$  to  $43^\circ 56.2'S$  and  $70^\circ 04.7'W$  to  $86^\circ 48.4'W$ , which is covered by satellite data. BIAS and RMSE were carried out as part of the spatial comparison of QuikSCAT and WRF data on wind magnitude.

#### 2.6. Analysis of the time-frequency domain

The wind magnitude and direction signals present a wide range of dominant frequencies. Requiring a tool that can break down the space-time-frequency series to determine the dominant modes of variability and how these modes vary over time, we used the wavelet transform (Torrence and Compo, 1998). The cross wavelet transform and wavelet phase coherence analysis were calculated following the methodology of Grinsted et al. (2004) to compare the time series of the simulations to the WRF and WKB measurements and identify the common frequency bands and intervals. The level of significance of the coherence wavelet was determined by the Monte Carlo method.

Given the above, the selection of a base wavelet is important. As like other investigations, we employed the Morlet wavelet (Avdakovic et al., 2011), which consists of a complex exponential multiplied by a Gaussian window. A non-dimensional frequency of  $w_0 = 6$  was used for this study (Torrence and Webster, 1999). The Morlet Wavelet provided a

good balance between time and frequency (Grinsted et al., 2004). Wind magnitude and direction were analyzed in this selection based on *in situ* observations and modeled data with boundary conditions that better adjust the buoy and satellite data. The analysis covers 3 months, from August 21 to November 21, 2009 to verify the behavior of the model at the synoptic (3 to 10 days) and sub-monthly scales (10–30 days).

### 3. Results

The model outputs and the satellite and buoy data were represented as roses of winds to characterize the wind regime in the study area (Fig. 3). The bars indicate wind direction.

Winds in central coastal Chile (Valparaíso) are predominantly southerly, representing over 70% of registered winds, while the magnitude tends to exceed  $10 \text{ ms}^{-1}$  in 25% of the *in situ* measurements. The percentages were higher in both cases in all the models. As well, there was a lower probability of winds from the first or second quadrant in the WKB data (close to 10%) and fewer incidence of intense winds (no  $> 4\%$  in any model). Intense winds were mainly from continent owing to low pressure fronts that approached from the north of incidence. The satellite data were from two daily measurements (in the morning and at night), which allowed for visualizing the daily wind cycle. The wind intensities and incidence of direction are similar to those registered by the WKB. These results show that coastal winds tend to be aligned with the orientation of the coast. The wind direction data indicate favorable conditions for upwelling during most of the analyzed period.

Wind magnitude and direction data from the different databases were analyzed separately to compare the databases. The wind magnitude data from the buoys and the model outputs were adjusted to a Weibull distribution to analyze the variability among the databases and assess simulated wind (Fig. 4). Weibull distribution has been used to represent the distribution of wind intensity because of its simplicity and good adjustment (Carvalho et al., 2013, Otero and Ruiz-Villareal, 2008).

The all simulations have similar distribution, distinct from that coming from buoy. The model tends to overestimate the occurrence of winds of  $< 7\text{--}8 \text{ ms}^{-1}$ , and underestimate the magnitude of winds that exceed  $14 \text{ ms}^{-1}$ . Table 2 shows the Weibull type parameters ( $\kappa$ ), which indicates the broadness of the distribution that determines the shape of the curve, the parameter of scale ( $\lambda$ ), which controls the development of the curve toward higher velocities and the most commonly occurring wind velocity ( $W_m$ ). The best statistical results will be marked in bold in the following tables.

The values for the WKB shape and scale parameters were respectively 2.41 and  $8.49 \text{ ms}^{-1}$ , while the corresponding modeled values were over 3 and  $9 \text{ ms}^{-1}$ . The modeling with ERA-Interim boundary conditions had the closest values to those of *in situ* measurements. The most common wind velocity for the different databases ranged between  $7.5$  and  $8.5 \text{ ms}^{-1}$ , which indicates that strong breezes are normal in this area.

Table 3 shows the data for the RMSE, BIAS and the correlation coefficient (R) for wind magnitudes compared to the models with different boundary conditions and with the QuikSCAT satellite data. It should be noted that the simulation data had a one-hour interval, while the satellite made two measurements daily (every 12 h).

The ERA-Interim-driven simulations were the closest to the BWK wind magnitude measurements. Grid 1 yielded the lowest RMSE and BIAS values, while Grids 2 and 3 yielded values similar to R. Comparing the buoy and satellite data yielded an R of 0.93, while the RMSE and BIAS were lower than those of the WRF simulations.

A more detailed analysis was carried out with four categories of

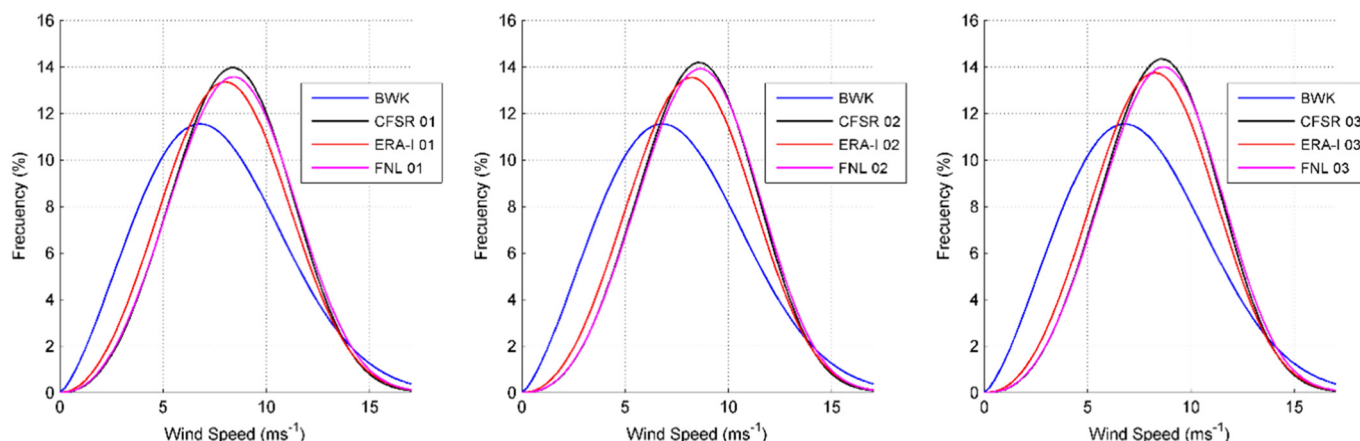


Fig. 4. Occurrence of wind velocity for the WKB and different grid sizes and WRF simulations, adjusted to Weibull distribution.

**Table 2**  
Parameters of shape ( $\kappa$ ), and scale ( $\lambda$ ) and the most common wind magnitudes ( $W_m$ ) representing Weibull distribution.

Buoy	Database	Grid	$\kappa$	$\lambda$ (ms <sup>-1</sup> )	$W_m$ (ms <sup>-1</sup> )	
Valparaíso	WKB		2.41	8.49	7.53	
		NCEP-CFSR	1	3.36	9.31	8.36
			2	3.48	9.46	8.51
	3		3.52	9.45	8.51	
	ERA-Interim	1	<b>3.11</b>	<b>9.07</b>	<b>8.12</b>	
		2	3.21	9.22	8.26	
		3	3.27	9.23	8.27	
	NCEP-FNL	1	3.29	9.39	8.42	
		2	3.45	9.54	8.58	
		3	3.47	9.55	8.59	

Bold data indicates significant the best results between the model and the data in situ.

**Table 3**  
Statistical of the comparison between WKB, WRF and QSCAT wind speed.

Wind speed (ms <sup>-1</sup> )	Dataset	Grid	RMSE	BIAS	R	
Buoy Valparaíso	NCEP-CFSR	1	2.41	0.83	0.75	
		2	2.48	0.98	0.74	
		3	2.49	0.98	0.74	
	ERA-Interim	1	<b>2.14</b>	<b>0.59</b>	0.79	
		2	2.16	0.73	<b>0.80</b>	
		3	2.16	0.74	<b>0.80</b>	
	NCEP-FNL	1	2.39	0.89	0.76	
		2	2.44	1.04	0.76	
		3	2.45	1.06	0.76	
	QuikSCAT			<b>1.25</b>	<b>0.06</b>	<b>0.93</b>

Bold data indicates significant the best results between the model and the data in situ.

**Table 4**  
Statistical comparison of the wind magnitude data of the different models to those of the WRF and WKB.

Wind speed bins	Buoy	Dataset	Grid	< 4 ms <sup>-1</sup>		4–8 ms <sup>-1</sup>		8–12 ms <sup>-1</sup>		> 12 ms <sup>-1</sup>	
				RMSE	BIAS	RMSE	BIAS	RMSE	BIAS	RMSE	BIAS
Valparaíso	NCEP-CFSR	1		3.92	2.92	2.45	1.04	1.38	<b>0.01</b>	1.39	-0.86
		2		4.09	3.12	2.50	1.20	1.38	0.12	1.31	-0.72
		3		4.11	3.15	2.50	1.23	1.39	0.11	1.39	-0.81
	ERA-Interim	1		<b>3.42</b>	<b>2.30</b>	<b>2.08</b>	<b>0.79</b>	1.36	-0.09	1.44	-0.85
		2		3.50	2.42	2.11	0.98	1.33	0.05	1.40	-0.80
		3		3.50	2.46	2.11	1.01	<b>1.32</b>	0.04	1.48	-0.85
	NCEP-FNL	1		3.88	2.71	2.41	1.20	1.42	0.12	1.29	-0.73
		2		4.00	2.93	2.44	1.35	1.43	0.25	<b>1.25</b>	<b>-0.65</b>
		3		4.03	2.97	2.44	1.37	1.44	0.25	1.34	-0.68

Bold data indicates significant the best results between the model and the data in situ.

wind magnitude, namely, < 4 ms<sup>-1</sup>, between 4 and 8 ms<sup>-1</sup>, between 8 and 12 ms<sup>-1</sup>, and over 12 ms<sup>-1</sup>. Table 4 shows the RMSE and BIAS calculated for the intervals. The wind magnitude categories are classified according to the buoy measurements.

The simulations yielded similar results for wind magnitude, with the ERA-Interim giving the best results. The positive BIAS of wind magnitude indicates overestimation of the model compared to buoy data, while the high RMSE values indicate a major model error compared to the *in situ* measurements. The RMSE and BIAS were high for the interval of < 4 ms<sup>-1</sup>. The RMSE and BIAS were low for the interval between 8 and 12 ms<sup>-1</sup>, the simulations made underestimations for the interval of > 12 ms<sup>-1</sup>.

Variability in wind direction was analyzed taking into account the differences between the WRF simulations and the WKB. Fig. 5 shows the dependence of differences in wind direction between the WRF simulations and the WKB. As can be seen, the majority of points are located between -45° and 45°. Most of the differences are for velocities under 6 ms<sup>-1</sup>. Negative values indicate clockwise rotation and positive value anticlockwise rotation of the simulations with respect to the buoy.

Comparing wind direction, the ERA-Interim-driven simulations most closely approximated the buoy data in relation to the RMSE and R, in particular for Grid Three (Table 5). The NCEP-FNL analysis had the lowest BIAS. The NCEP-CFSR-forced simulation had the poorest performance for wind direction. The directional data from the satellite had the highest BIAS, of 8.25°, and R of 0.83.

An analysis was also carried out involving four intervals (Table 6) east (between 45° and 135°), south (between 135° and 225°), west (between 225° and 315°) and north (between 315° and 45°), a comparison that is classified according to the wind directions measured by the buoy. In terms of the RMSE and BIAS, the ERA-Interim-driven

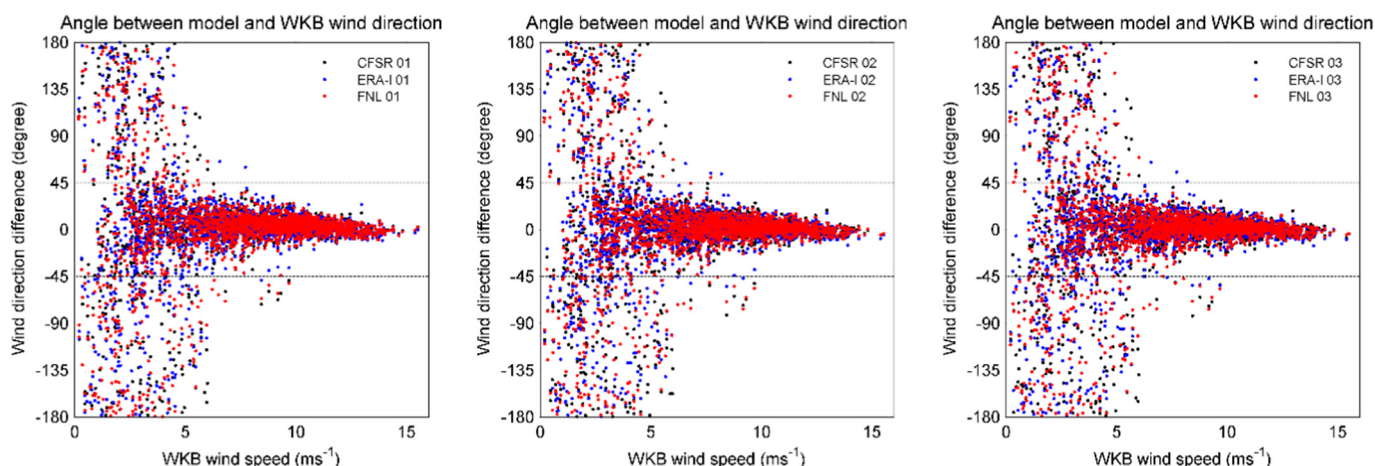


Fig. 5. Dependence of the differences in wind direction between the WRF simulations and the WKB, with wind magnitude from the buoy.

**Table 5**  
Statistical of the comparison between WKB, WRF and QSCAT wind direction.

Wind directions (°)	Database	Grid	RMSE	BIAS	R
Buoy Valparaíso	NCEP-CFSR	1	44.45	2.81	0.81
		2	45.33	2.29	0.81
		3	45.08	2.03	0.81
	ERA-Interim	1	41.41	1.74	0.83
		2	41.01	0.45	<b>0.84</b>
		3	<b>40.88</b>	0.46	<b>0.84</b>
	NCEP-FNL	1	43.59	0.60	0.82
		2	43.70	0.43	0.82
		3	43.84	-0.01	0.82
QuikSCAT			41.98	8.25	0.83

Bold data indicates significant the best results between the model and the data in situ.

simulations are the most similar to the buoy data, with the exception of westerly winds, where Grid 1 of the NCEP-CFSR has slightly lower RMSE and BIAS. All the simulations agree adequately with buoy measurements for winds from the south and west, but do not adequately represent winds from the north and east.

These results show that the QuikSCAT wind intensity data generally well represents the WKB wind magnitude data. Given the above, wind magnitude in the QuikSCAT data and the WRF simulations for Grid 1 were analyzed spatially (Figs. 6 and 7).

The highest BIAS values (approximately  $1.5 \text{ ms}^{-1}$  for the NCEP-FNL) were for the coast and the northern part of the study area, which indicates that the model tends to underestimate for the coast, while the estimations for the open sea are more accurate (Fig. 6). The NCEP-FNL overestimates wind intensity at the northern end of the study area, while it underestimates it at the southern end. For its part, the ERA-

**Table 6**  
Statistical comparison of the models and the WRF and WKB for wind direction.

Wind direction bins			North		East		South		West	
Buoy	Dataset	Grid	RMSE	BIAS	RMSE	BIAS	RMSE	BIAS	RMSE	BIAS
Valparaíso	NCEP-CFSR	1	130.5	-50.7	112.3	63.7	17.8	4.0	<b>59.1</b>	<b>-35.7</b>
		2	133.3	-43.2	113.2	68.9	18.3	2.7	61.4	-37.8
		3	133.7	-52.8	111.7	67.3	17.7	3.1	63.4	-39.0
	ERA-Interim	1	114.8	-44.3	110.8	36.8	<b>15.5</b>	4.3	59.9	-37.8
		2	111.0	<b>-35.9</b>	109.1	<b>30.2</b>	<b>15.5</b>	2.9	63.5	-39.2
		3	<b>110.6</b>	-41.7	<b>108.6</b>	34.8	16.0	2.9	61.8	-38.8
	NCEP-FNL	1	121.4	-63.2	112.0	39.0	18.0	3.9	63.4	-37.9
		2	121.6	-55.0	112.1	44.6	17.6	2.9	66.0	-38.5
		3	121.5	-54.6	112.9	41.9	17.3	<b>2.6</b>	67.7	-39.7

Bold data indicates significant the best results between the model and the data in situ.

Interim overestimates intensity along the coast and underestimates it in the open sea, while the configuration of the NCEP-CFSR is similar to that of the NCEP-FNL.

The highest RMSE values were for the close to the coast, the NCEP-FNL values being over  $2.5 \text{ ms}^{-1}$ . The most similar wind intensities between what was registered by the satellite and the models was for offshore winds, although this was not the case for the NCEP-CFSR model, which had significant errors for offshore winds in the southern part of the study area. The ERA-Interim-driven simulation most approximated the QuikSCAT measurements.

Coherence and phase wavelets (Fig. 8) of the complex vectors ( $w = u + vi$ ) obtained from the wind magnitude and direction series were analyzed. The WKB measurements were compared to the Grid 1 results of the WRF with distinct boundary conditions. This grid was chosen because it generally yielded the best results to the basic statistics, mainly in relation to wind magnitude.

Fig. 7 shows that the vectors indicate the phase difference in the *in situ* measurements and the modeling results. If the vector is heading to the right, the angle is  $0^\circ$  and the series is in phase, while if it is heading to the left, the angle is  $180^\circ$  and the series is out of phase, upward pointing indicates  $90^\circ$  and downward  $-90^\circ$ . Only the Grid 1 wavelets of different conditions are shown, as the rest were similar.

The coherence and phase wavelets had similar results. Coherence was not significant for periods shorter than a day, except for particular periods. The time series were generally in phase for the one-day band and coherence was significant, except for the periods September 11 to 13 and October 30 to November 2.

The series are significant at the synoptic scale in almost all the simulations. However, the results with ERA-Interim indicate that in addition to being significant, the simulations are in phase in most of the periods. The ERA-Interim simulation was more significant than the

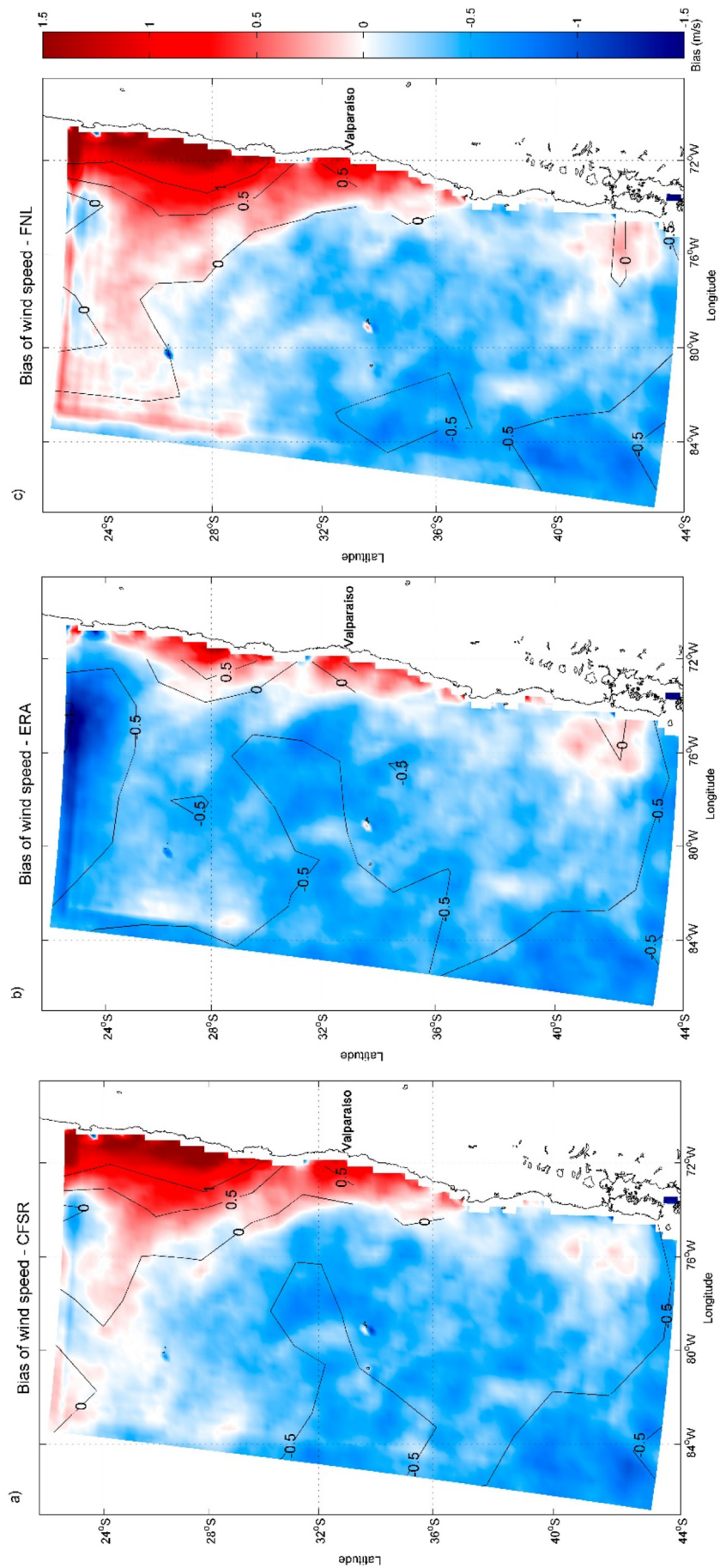


Fig. 6. Wind magnitude BIAS of QuikSCAT satellite and Grid 1 simulation driven by the a) NCEP-CFJR, b) ERA-Interim, and c) NCEP-FNL.

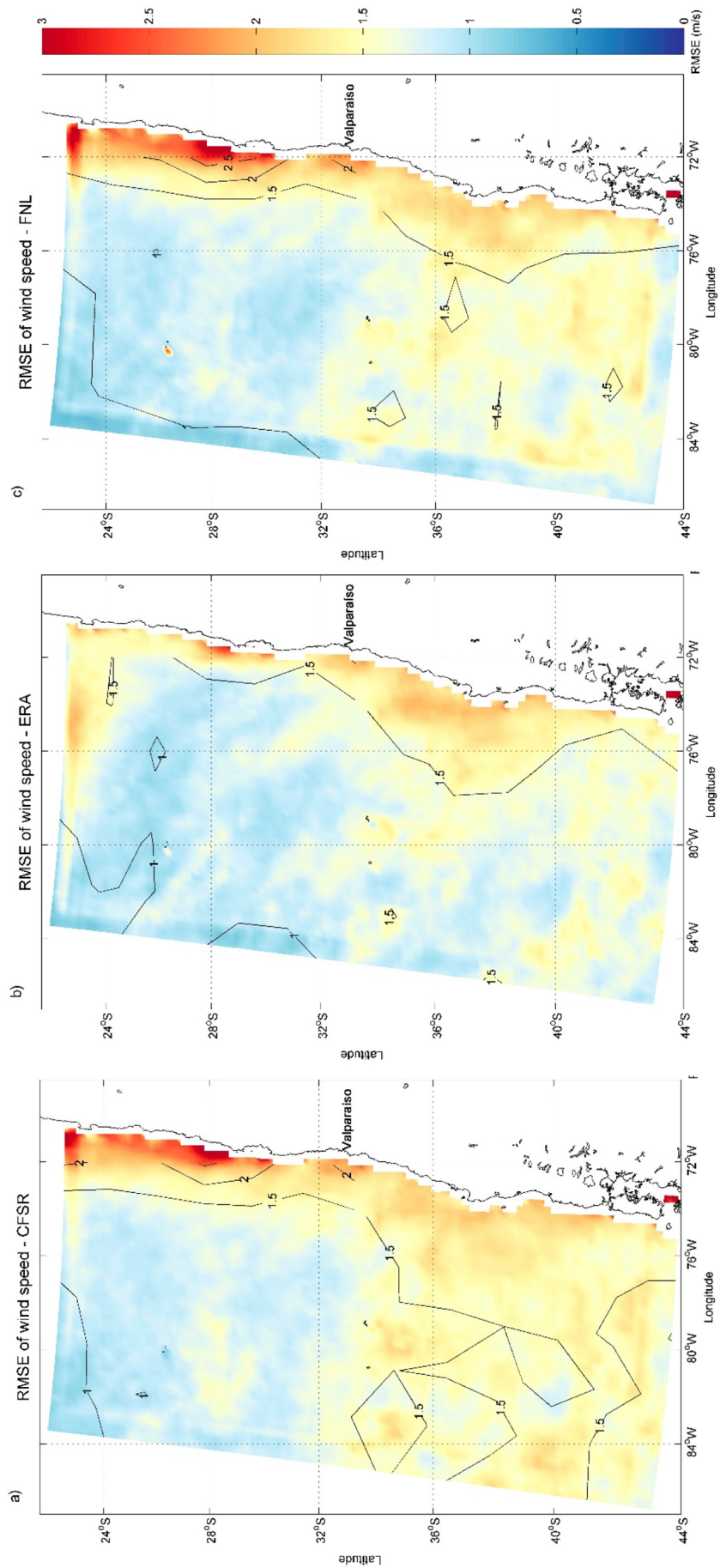


Fig. 7. The wind magnitude RMSE of QuikSCAT data and the Grid 1 simulations driven by the a) NCEP-CFSR, b) ERA-Interim, and c) NCEP-FNL.

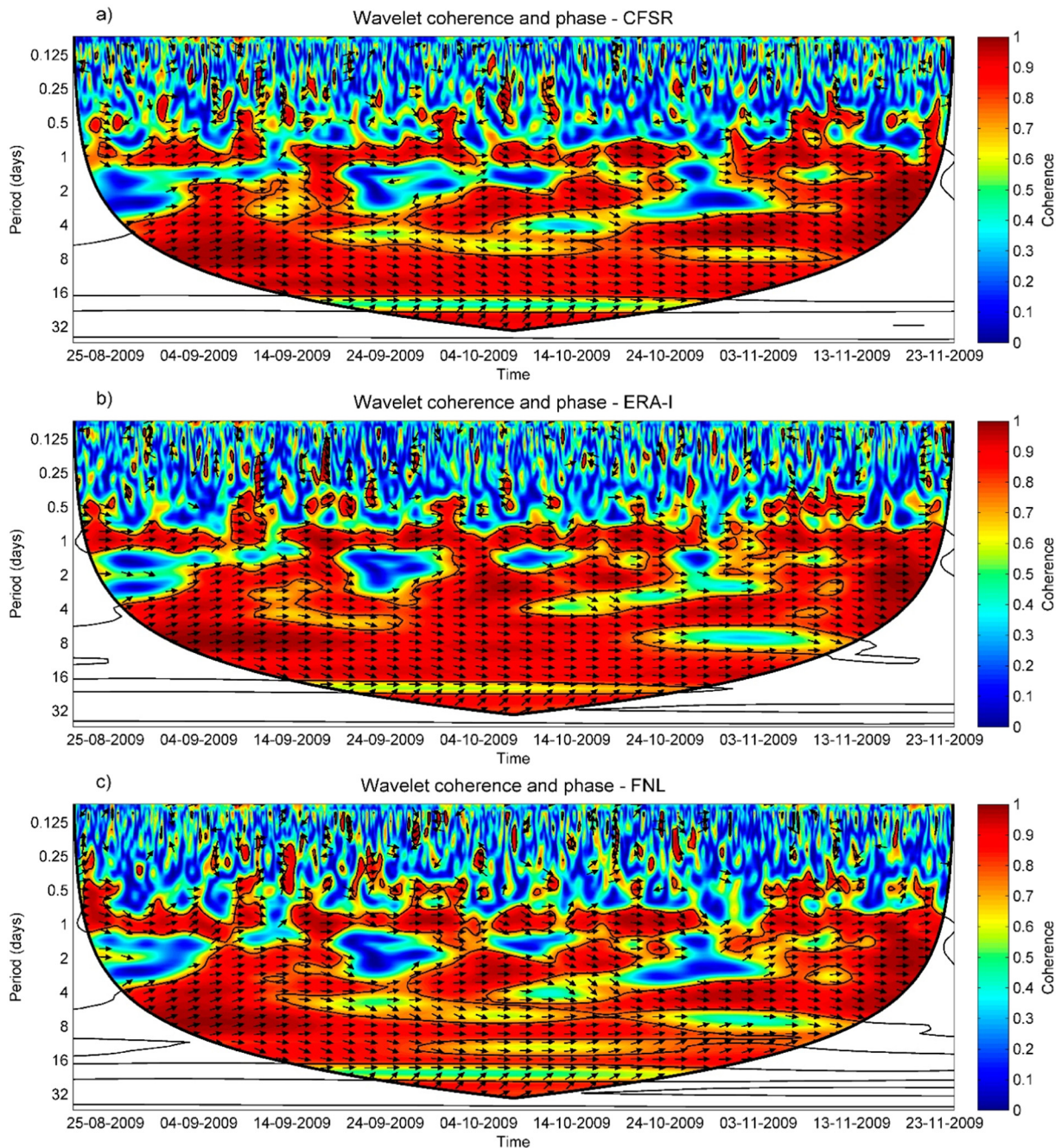


Fig. 8. Coherence and phase wind wavelets of the WKB and the Grid 1simulation driven by the a) NCEP-CFSR, b) ERA-Interim, and c) NCEP-FNL.

other boundary conditions for the sub-monthly band. The phase angle in all the wavelets was close to  $45^\circ$ , which indicate that the WRF model shifts between 2 and 3 days for this band.

#### 4. Discussion

Several authors have noted the predominance of winds from the third quadrant (Pizarro et al., 1994; Mattar and Borvarán, 2016) as observed with coastal stations. Tiemann et al. (1983) and Naveas (2007) installed anemometers at Punta Curaumilla (Fig. 1), coinciding with the predominance of southerly winds with intensities similar to those registered by the WKB. These winds are favorable to coastal upwelling, presenting their greatest intensity, along the coast of Chile ( $18^\circ$  to  $42^\circ$  S), during the spring and summer months (Bakun and Nelson, 1991).

We think that a model based offshore wind study could provide vital information for the renewable energy community. Mattar and Guzmán-Ibarra, 2017 studied the offshore wind energy potential using 10 m wind from ERA-Interim between 1979 and 2015, a product with a  $0.125^\circ$  resolution, and extrapolated the 10 m wind results to a height of 140 m using a logarithmic approach. A study of the offshore wind profile could be better addressed with a high vertical resolution modeling study. Since 2009 technological solution to address this issue is a buoy mounted lidar sensor (Pichugina et al., 2012; Gottschall et al., 2017), which is can be a better, although more costly, alternative to numerical models to estimate offshore wind potential. A modeling approach could be used beforehand to select deployment areas for the buoy based lidar instrument.

The QuikSCAT V3L2B12 database (Fore et al., 2013) on wind intensity is similar to what is registered by the WKB, with RMSE

( $1.25 \text{ ms}^{-1}$ ) and BIAS values ( $0.06 \text{ ms}^{-1}$ ) similar to those cited by other sources (Ebuchi et al., 2002; Pickett, 2003). However, previous studies excluded low intensity winds, rainy periods and data from buoys near the coast. Comparing our results to those of earlier studies, there has been an improvement in QuikSCAT wind direction data.

The WRF model simulations generally overestimated wind intensity compared to the WKB measurements. A more detailed analysis of magnitude intervals (Table 4) indicates that low intensity winds ( $< 4 \text{ ms}^{-1}$ ) are significantly overestimated, while for intermediate intensity (from 4 to  $12 \text{ ms}^{-1}$ ), the tendency to overestimate is attenuated. As well, the best performance of the models is in this interval, which concurs with the results of Carvalho et al. (2012). The simulations underestimated wind intensity ( $> 12 \text{ ms}^{-1}$ ), which could be due to inaccurate *in situ* measurements (Large et al., 1995) given that there are heavy waves in the periods with strong winds, which can cause the buoys to shift position and oscillate.

WRF is a mesoscale model, capable of representing spatial scales ranging from 2 to 2,000 km, and temporal scales from minutes to a few days (Orlanski, 1975), being able to represent phenomena such as convective storms, coastal tidal, sea breeze and cyclones tropical bordering the synoptic scale. However, there are phenomena that, despite being included in the mesoscale, are not capable of being represented by the Global Models that provide boundary conditions to the WRF Regional Model.

Global models have a lower spatial resolution in relation to topography, a large area of land is represented by the value of the same point. This implies that there are phenomena that are not going to be represented in the wind fields or are less important. Being close to the continent, the wind fields will have complex spatial structures that are generated by the interactions with the topography (Perlin et al., 2004). A dependence analysis (Fig. 5) indicates that the model better simulates the real direction of winds when they are stronger than  $6 \text{ ms}^{-1}$ . However, it can be appreciated from the direction interval RMSE and BIAS (Table 6) that unlike winds from the south and west, winds from north and east (Fig. 3) are not well represented by the simulations. Other researchers have indicated that the WRF model tends to be less precise when winds come from the land (Carvalho et al., 2012). However, the directions by the simulations continue to be more precise than those in QuikSCAT data.

It is estimated that the QuikSCAT wind magnitude data provides a good representation of the winds measured by the WKB. A statistical spatial analysis was made of the differences between satellite data and simulation results (Figs. 6 and 7). The major differences were in the coastal area, which could be due to the masking effect of the continent, which negatively affects satellite information (Furevik et al., 2010), the irregular discretization of the topographic mesh used by the WRF model (Sousa et al., 2013) or that the model is unable to capture due weak synoptic processes (Penabad et al., 2008).

Wavelet coherence and phase analysis is sensitive to the differences between the different time series, although the correlation coefficients are close to 0.8 (Table 3). This demonstrates that it is difficult for the WRF model to automatically characterize high frequencies (hourly data). However, atmospheric processes close to the period of 1 day or longer are characterized quite well, such as the sea breeze (figure not shown). Apparently the model has a hard time reproducing the low magnitude winds that come from the continent. Garreaud et al. (2002) indicates that winds from the east are known as coastal trough, coinciding with information recorded by the buoy and not simulated by the model or masked by the winds from the south that are overestimated and subtracting their respective importance.

The ERA-Interim boundary condition was the statistical analysis that yielded the most similar results to the observed buoy and satellite wind data, which agrees with Carvalho et al. (2012) in relation to the Portuguese coast. The analysis showed that simulating with higher spatial resolution does not necessarily improve the results. Finally, although this work was focused identifying the boundary condition that

best adjusted to the central Chile, the physical parametrization can significantly affect the results of the model (Mattar and Borvarán, 2016), and consider a higher spatial resolution of SST as it is a sector so close to the coast, being able to improve model results.

## 5. Conclusions

Oceanic surface winds in the central Chile can be simulated by WRF mesoscale atmospheric modeling, forced by different boundary conditions (analysis or reanalysis). Because of the diversity of boundary conditions, this work aimed to compare a series of model results with *in situ* measurements and satellite information for the central coast of Chile using NCEP-CFSR and ERA-Interim reanalysis and NCEP-FNL analysis data.

The results of surface wind simulations were compared to the wind data from the ODAS buoy and the QuikSCAT to determine firstly which database results in the most accurate wind simulations and secondly whether increasing the spatial resolution results in more accurate simulations. The main conclusions are:

- All the simulations and the *in situ* measurements indicate the predominance of southern winds, which are favorable for upwelling. Over 25% of simulated winds have a magnitude of  $> 10 \text{ ms}^{-1}$ , and almost 4% come from the continent, owing to low pressure fronts that come from the north. In the latter case, the percentages of the *in situ* data were higher.
- The modeling tends to simulate winds of intermediate intensity (from 4 to  $12 \text{ ms}^{-1}$ ) more accurately, with fewer errors and only slight overestimation. There are more errors and greater overestimation with weak winds ( $< 4 \text{ ms}^{-1}$ ), while there are few errors with strong winds ( $> 12 \text{ ms}^{-1}$ ) and the winds tend to be underestimated.
- The wind directions showed that in instances where the wind intensities are equal to or  $> 6 \text{ ms}^{-1}$ , the model best reflects the wind directions. However, wind directions are not well represented when there are winds from the continent.
- From the spatial analysis of wind intensity, between the simulations and satellite data, major errors and overestimation of the model will occur in the coastal sectors, while the frequently affected ocean area where the errors are fewer and slight underestimation.
- The Wavelet coherence and phase analysis determined that there is no significant coherence for winds in periods of less than the daily cycle, while there is good coherence for winds in the period daily and they are in phase. However, there are phenomena at the synoptic and sub-monthly scales that are not being simulated by the model. The synoptic and sub-monthly scales are highly coherent, the former in phase and the latter out of phase by two to 3 days.

This study indicates that the ERA-Interim is the boundary condition model that obtains the most coherent results for ocean surface winds. Other boundary conditions like the NCEP-FNL and NCEP-CFSR, are valid alternatives for modeling winds. We also concluded that increasing spatial resolution does not significantly improve the results of the model.

## Acknowledgements

We are grateful to the Hydrographic and Oceanographic Service of the Chilean Navy for facilitating the wind measurements from the WatchKeeper buoy. This research was supported by the super-computing infrastructure of the NLHPC (ECM-02).

## References

- Aguilera, V., Escribano, R., Herrera, L., 2009. High frequency responses of nanoplankton and microplankton to wind-driven upwelling off northern Chile. *J. Mar. Syst.* 78 (1),

- 124–135.
- Aguirre, C., Garreaud, R.D., Rutllant, J.A., 2014. Surface ocean response to synoptic-scale variability in wind stress and heat fluxes off south-central Chile. *Dynamics of Atmospheres and Oceans* 65, 64–85. <https://doi.org/10.1016/j.jdynatmoce.2013.11.000>.
- Álvarez, I., Gomez-Gesteira, M., deCastro, M., Carvalho, D., 2014. Comparison of different wind product and buoy wind data with seasonality and interannual climate variability in the southern Bay of Biscay (2000–2009). *Deep-Sea Research II* 106, 38–48. <https://doi.org/10.1016/j.dsr2.2013.09.028>.
- Ancapichún, S., Garcés-Vargas, J., 2015. Variability of the southeast Pacific subtropical anticyclone and its impact on sea surface temperature off north-central Chile. *Ciencias Marinas* 41 (1), 1–20. <https://doi.org/10.7773/cm.v41i1.2338>.
- Avdakovic, A., Lukac, A., Nuhanovic, A., Music, M., 2011. Wind speed data analysis using Walevel transform. *International Journal of Environmental, Chemical, Ecological, Geological and Geophysical Engineering* 5 (3), 138–142.
- Bakun, A., Nelson, C.S., 1991. The seasonal cycle of wind-stress curl in subtropical eastern boundary current regions. *Journal of Physical Oceanographic* 21 (12), 1815–1834.
- Balzarini, A., Pirovano, G., Riva, G.M., Toppetti, A., Bozzano, R., Pensieri, S., Canepa, E., Schiano, E., 2011. WRF evaluation exercise using open sea in situ measurements and land coastal data. In: *4th Conference on Harmonisation within Atmospheric Dispersion Modelling for Regulatory Purpose (335–339)*. Meso-scale Meteorology and Air Quality Modelling, Kos, Greece.
- Bengtsson, L., Arkin, P., Berrisford, P., Folland, C.K., Gordon, C., Haines, K., Hodges, K.I., Jones, P., Kallberg, P., Rayner, N., Simmons, A.J., Stammer, D., Thorne, P.W., Uppala, S., Vose, R.S., 2007. The Need for a Dynamical Climate Reanalysis. *Bull. American Meteorological Society*, pp. 495–501.
- Berens, P., 2009. CircStat: a MATLAB toolbox for circular statistics. *Journal of Statistical Software* 31 (10), 1–21.
- Caires, S., Sterl, A., Bidlot, J.-R., Graham, N., Swail, V., 2004. Intercomparison of different wind-wave reanalyses. *Journal of Climate* 17 (10), 1893–1913. [https://doi.org/10.1175/1520-0442\(2004\)017<1893:IODWR>2.0.CO;2](https://doi.org/10.1175/1520-0442(2004)017<1893:IODWR>2.0.CO;2).
- Capet, J.X., Marchesiello, P., McWilliams, J.C., 2004. Upwelling response to coastal wind profiles. *Geophys. Res. Lett.* 31, L13311. <https://doi.org/10.1029/2004GL020123>.
- Carvalho, D., Rocha, A., Gómez-Gesteira, M., 2012. Ocean surface wind simulation forced by different reanalyses: comparison with observed data along the Iberian Peninsula coast. *Ocean Model.* 56, 31–42. <https://doi.org/10.1016/j.ocemod.2012.08.002>.
- Carvalho, D., Rocha, A., Gómez-Gesteira, M., Alvarez, I., Silva Santos, C., 2013. Comparison between CCMP, QuikSCAT and buoy winds along the Iberian Peninsula coast. *Remote Sens. Environ.* 137, 173–183. <https://doi.org/10.1016/j.rse.2013.06.005>.
- Carvalho, D., Rocha, A., Gómez-Gesteira, M., Silva Santos, C., 2014. Offshore wind energy resource simulation forced by different reanalyses: comparison with observed data in the Iberian Peninsula. *Appl. Energy* 134, 57–64. <https://doi.org/10.1016/j.apenergy.2014.08.018>.
- Dee, D.P., Uppala, S.M., Simmons, A.J., Berrisford, P., Poli, P., Kobayashi, S., Andrae, U., Balmaseda, M.A., Balsamo, G., Bauer, P., Bechtold, P., Beljaars, A.C.M., Van de Berg, L., Bidlot, J., Bormann, N., Delsol, C., Dragani, R., Fuentes, M., Geer, A.J., Haimberger, L., Healy, S.B., Hersbach, H., Hólm, E.V., Isaksen, I., Källberg, P., Köhler, M., Matricardi, M., McNally, A.P., Monge-Sanz, B.M., Morcrette, J.-J., Park, B.-K., Peubey, C., de Rosnay, P., Tavaloto, C., Thépaut, J.-N., Vitart, F., 2011. The ERA-Interim reanalysis: configuration and performance of the data assimilation system. *Q. J. R. Meteorol. Soc.* 137, 553–597. <https://doi.org/10.1002/qj.828>.
- Ebuchi, N., Graber, H.C., Caruso, M.J., 2002. Evaluation of wind vectors observed by QuikSCAT/sea winds using ocean buoy data. *Journal of Atmospheric Oceanic Technology* 19, 2049–2062. [https://doi.org/10.1175/1520-0426\(2002\)019<2049:EOWVOB>2.0.CO;2](https://doi.org/10.1175/1520-0426(2002)019<2049:EOWVOB>2.0.CO;2).
- Fairall, C.W., Bradley, E.F., Hare, J.E., Grachev, A.A., Edson, J., 2003. Bulk parameterization of air-sea fluxes: updates and verification for the COARE algorithm. *Journal of Climate* 16, 571–591. [https://doi.org/10.1175/1520-0442\(2003\)016<0571:BPOASF>2.0.CO;2](https://doi.org/10.1175/1520-0442(2003)016<0571:BPOASF>2.0.CO;2).
- Fore, A.G., Stiles, B.W., Chau, A.H., Williams, B.A., Dumber, R.S., Rodríguez, E., 2013. Point-wise wind retrieval and ambiguity removal improvements for the QuikSCAT climatological data set. *IEEE Trans. Geosci. Remote Sens.* 52 (1), 51–59. <https://doi.org/10.1109/TGRS.2012.2235843>.
- Furevik, B.R., Sempreviva, A.M., Cavalieri, L., Lefèvre, J.-M., Tranter, C., 2010. Eight years of wind measurements from scatterometer for wind resource mapping in the Mediterranean Sea. *Wind Energy* 14 (3), 355–372. <https://doi.org/10.1002/we.425>.
- Garreaud, R., Rutllant, J., Fuenzalida, H., 2002. Coastal lows in north-central Chile: mean structure and evolution. *Mon. Wea. Rev.* 130, 75–88.
- Garreaud, R.D., Aceituno, P., 2001. Chapter 2: atmospheric circulation over South America: Mean features and variability. In: Veblen, E.T., Young, K., Orme, A. (Eds.), *The Physical Geography of South America*. University Press, Oxford, pp. 1–33.
- Garreaud, R.D., Muñoz, R., 2005. The Low-level jet off the west coast of subtropical South America: structure and variability. *Monthly Weather Review* 133, 2246–2261. <https://doi.org/10.1175/MWR2972.1>.
- Gottschall, J., Gribben, B., Stein, D., Würth, I., 2017. Floating lidar as an advanced offshore wind speed measurement technique: current technology status and gap analysis in regard to full maturity. *Wiley Interdisciplinary Reviews: Energy and Environment* 6 (5), e250.
- Grinsted, A., Moore, J.C., Jevrejeva, S., 2004. Application of the cross wavelet transform and wavelet coherence to geophysical time series. *Nonlinear Processes in Geophysics* 11, 561–566. <https://doi.org/10.5194/npg-11-561-2004>.
- Herrera, L., Escribano, R., 2006. Factors structuring the phytoplankton community in the upwelling site off El Loa River in northern Chile. *J. Mar. Syst.* 61 (1–2), 13–38.
- Large, W.G., Morzel, J., Crawford, G.B., 1995. Accounting for Surface Wave Distortion of the Marine Wind Profile in Low-Level Ocean Storms Wind Measurements. *Journal of Physical Oceanography* 25, 2959–2971. [https://doi.org/10.1175/1520-0485\(1995\)025<2959:AFSWDO>2.0.CO;2](https://doi.org/10.1175/1520-0485(1995)025<2959:AFSWDO>2.0.CO;2).
- Letelier, J., Pizarro, O., Nuñez, S., 2009. Seasonal variability of coastal upwelling and the upwelling front off central Chile. *Journal of Geophysical Research* 114, C12009. <https://doi.org/10.1029/2008JC005171>.
- Luo, W., Taylor, M.C., Parker, S.R., 2008. A comparison of spatial interpolation methods to estimate continuous wind speed surfaces using irregularly distributed data from England and Wales. *Int. J. Climatol.* 28, 947–959. <https://doi.org/10.1002/joc.1583>.
- Mattar, C., Borvarán, D., 2016. Offshore wind power simulation by using WRF in the central coast of Chile. *Renewable Energy* 94, 22–31. <https://doi.org/10.1016/j.renene.2016.03.005>.
- Mattar, C., Guzmán-Ibarra, M.C., 2017. A techno-economic assessment of offshore wind energy in Chile. *Energy* 133, 191–205.
- Muñoz, R., 2008. Diurnal cycle of surface winds over the subtropical southeast Pacific. *J. Geophys. Res.* 113, 1–15. <https://doi.org/10.1029/2008JD009957>.
- Naveas, C., 2007. Height Extrapolation of wind speed, experimental and comparative analysis. In: *6th International Conference on Sustainable Energy Technologies*, pp. 1–6 (Santiago de Chile).
- Orlanski, I., 1975. A rational subdivision of scales for atmospheric processes. *Bull. Am. Meteorol. Soc.* 527–530.
- Otero, P., Ruiz-Villareal, M., 2008. Wind forcing of the coastal circulation off north and northwest Iberia: comparison of atmospheric models. *Journal of Geophysical Research* 113, 1–30. <https://doi.org/10.1029/2008JC004740>.
- Penabad, E., Alvarez, I., Balseiro, C.F., deCastro, M., Gómez, B., Pérez-Muñuzuri, V., Gómez-Gesteira, M., 2008. Comparative analysis between operational weather prediction models and QuikSCAT wind data near the Galician coast. *Journal of Marine Systems* 72, 256–270. <https://doi.org/10.1016/j.jmarsys.2007.07.008>.
- Pensieri, S., Bozano, R., Schiano, M.E., 2010. Comparison between QuikSCAT and buoy wind data in the Ligurian Sea. *Journal of Marine System* 81, 286–296. <https://doi.org/10.1016/j.jmarsys.2010.01.004>.
- Perlin, N., Samelson, R.M., Chelton, D.B., 2004. Scatterometer and model wind and wind stress in the Oregon-California coastal zone. *Mon. Wea. Rev.* 132, 2110–2129. [https://doi.org/10.1175/1520-0493\(2004\)132%3C2110:SAMWAW%3E2.0.CO;2](https://doi.org/10.1175/1520-0493(2004)132%3C2110:SAMWAW%3E2.0.CO;2).
- Pezza, A.B., Simmonds, I., Renwick, J.A., 2007. Southern Hemisphere cyclones and anticyclones: Recent trends and links with decadal variability in the Pacific Ocean. *International Journal of Climatology* 27, 1403–1419. <https://doi.org/10.1002/joc.1477>.
- Pichugina, Y.L., Banta, R.M., Brewer, W.A., Sandberg, S.P., Hardesty, R.M., 2012. Doppler lidar-based wind-profile measurement system for offshore wind-energy and other marine boundary layer applications. *J. Appl. Meteorol. Climatol.* 51 (2), 327–349.
- Pickett, M.H., Tang, W., Rosenfeld, L.K., Wash, C.H., 2003. QuikSCAT satellite comparisons with nearshore buoy wind data off the U.S. West Coast. *Journal of Atmospheric and Ocean Technology* 20, 1869–1879.
- Pizarro, O., Hormazábal, S., González, A., Yáñez, E., 1994. Variabilidad del viento, nivel del mar y temperatura en la costa norte de Chile. *Investigaciones Marinas* 22, 85–101. <https://doi.org/10.4067/S0717-71781994002200007>.
- Purba, N.P., Jaya, K., Muallimah, A., Dessy, T., Ghalib, K.G., Resti, A.I., Damanik, F.S., 2014. Preliminary Research of Using Ocean Currents and Wind Energy to Support Lighthouse in Small Island, Indonesia. *Energy Procedia* 47, 204–210. <https://doi.org/10.1016/j.egypro.2014.01.215>.
- Renault, L., Dewitte, B., Marchesiello, P., Illig, S., Echevin, V., Cambon, G., Ramos, M., Astudillo, O., Minnis, P., Ayers, J.K., 2012. Upwelling response to atmospheric coastal jets off central Chile: a modeling study of the October 2000 event. *J. Geophys. Res.* 117 (C02030), 1–21.
- Risien, C.M., Chelton, D.B., 2006. A Satellite-derived climatology of global ocean winds. *Remote Sensing of Environment* 105, 221–236. <https://doi.org/10.1016/j.rse.2006.06.017>.
- Ruti, P.M., Marullo, S., D'Ortenzio, F., Tremant, M., 2008. Comparison of analyzed and measured wind speeds in the perspective of oceanic simulations over the Mediterranean basin: Analyses, QuikSCAT and buoy data. *Journal of Marine Systems* 70, 33–48. <https://doi.org/10.1016/j.jmarsys.2007.02.026>.
- Rutllant, J.A., Garreaud, R.D., 2005. Capa Límite Marina en el Pacífico Suroriental Subtropical durante el Crucero CIMAR 5. *Ciencia y Tecnología Marina* 28 (1), 25–33.
- Rutllant, J.A., Rosenbluth, B., Hormazabal, S., 2004. Intraseasonal variability of wind-forced coastal upwelling off central Chile (30°S). *Continental Shelf Research* 24, 789–804. <https://doi.org/10.1016/j.csr.2004.02.004>.
- Saha, S., Moorthi, S., Pan, H., Wu, X., Wang, J., Nadiga, S., Tripp, P., Kistler, R., Woollen, J., Behringer, D., Liu, H., Stokes, D., Grubbin, R., Gayno, G., Wang, J., Hou, Y., Chuang, H., Juang, H., Sela, J., Iredell, M., Treardon, R., Kleist, D., Delst, P., Keyser, D., Derber, J., Ek, M., Meng, J., Wei, H., Yang, R., Lord, S., Dool, H., Kumar, A., Wang, W., Long, C., Chelliah, M., Xue, Y., Huang, B., Schemm, J.-K., Ebisuzaki, W., Lin, R., Xie, P., Chen, M., Zhou, S., Higgins, W., Zou, C.-Z., Liu, Q., Chen, Y., Han, Y., Cucurull, L., Reynolds, R.W., Rutledge, G., Goldberg, M., 2010. The NCEP climate forecast system reanalysis. *Bull. Am. Meteorol. Soc.* 1015–1057.
- Sánchez, R.F., Relvas, P., Pires, H.O., 2007. Comparisons of ocean scatterometer and anemometer winds off the southwestern Iberian Peninsula. *Continental Shelf Research* 27, 155–175. <https://doi.org/10.1016/j.csr.2006.09.007>.
- Skamarock, W. C., Klemp, J. B., Dudhia, J., Gill, D. O., Barker, D. M., Duda, M. G., Huang, X.-Y., Wang, W. and Powers, J. G. 2008. A description of the advanced research WRF version 3. NCAR Technical Note, NCAR/TN-475 + STR.
- Sousa, M.C., Alvarez, I., Vaz, N., Gómez-Gesteira, M., Dias, J.M., 2013. Assessment of Wind Pattern Accuracy from the QuikSCAT Satellite and the WRF Model along the Galician Coast (Northwest Iberian Peninsula). *Monthly Weather Review* 141, 742–753. <https://doi.org/10.1175/MWR-D-11-00361.1>.
- Stopa, J.E., Cheung, K.F., 2014. Intercomparison of wind and wave data from the ECMWF Reanalysis Interim and the NCEP Climate Forecast System Reanalysis. *Ocean*

- Modelling 75, 65–83. <https://doi.org/10.1016/j.ocemod.2013.12.006>.
- Tang, W., Liu, W.T., Stiles, B.W., 2004. Evaluation of High-Resolution Ocean Surface Vector Wind Measured by QuikSCAT Scatterometer in Coastal Regions. *IEEE Transactions on Geoscience and Remote Sensing* 42 (8), 1762–1769. <https://doi.org/10.1109/TGRS.2004.831685>.
- Tiemann, R., Naveas, C. and Rosas, J. 1983. Análisis estadístico del potencial eólico en la V región. *II Simposion Interuniversitario de energía*, (págs. 503–518). (Santiago de Chile).
- Torrence, C., Compo, G.P., 1998. A Practical Guide Wavelet Analysis. *Bulletin of the American Meteorological Society* 61–78. [https://doi.org/10.1175/1520-0477\(1998\)079<0061:APGTWA>2.0.CO;2](https://doi.org/10.1175/1520-0477(1998)079<0061:APGTWA>2.0.CO;2).
- Torrence, C., Webster, P.J., 1999. Interdecadal Changes in the ENSO-Monsoon System. *Journal of Climate* 12, 2679–2690. [https://doi.org/10.1175/1520-0442\(1999\)012<2679:ICITEM>2.0.CO;2](https://doi.org/10.1175/1520-0442(1999)012<2679:ICITEM>2.0.CO;2).
- Torres, R., Turner, D., Rutllant, J., Sobarzo, M., Antezana, T., Gonzalez, H.E., 2002. CO<sub>2</sub> outgassing off central Chile (31–30° S) and northern Chile (24–23° S) during austral summer 1997: the effect of wind intensity on the upwelling and ventilation of CO<sub>2</sub>-rich waters. *Deep-Sea Res. I Oceanogr. Res. Pap.* 49 (8), 1413–1429.
- Wallcraft, A.J., Kara, A.B., Barron, C.N., Metzger, E.J., Pauley, R.L., Bourassa, M.A., 2009. Comparisons of monthly mean 10 m wind speeds from satellites and NWP products over the global ocean. *Journal of Geophysical Research* D16109 (114), 1–14. <https://doi.org/10.1029/2008JD011696>.